8

Estimation of Tire-Road Forces and Vehicle Sideslip Angle

Guillaume Baffet[1], Ali Charara[2] and Daniel Lechner[3]
[1]*HEUDIASYC laboratory – CNRS (during this study)*
[1]*IRCCYN Laboratory, Ecole des Mines de Nantes – CNRS (Today)*
[2]*HEUDIASYC Laboratory, Universite de technologie de Compiegne – CNRS*
[3]*INRETS-MA laboratory*
France

1. Introduction

This chapter focuses on the estimation of car dynamic variables for the improvement of vehicle safety, handling characteristics and comfort. More specifically, a new estimation process is proposed to estimate longitudinal/lateral tire-road forces, velocity, sideslip angle and wheel cornering stiffness. One main contribution of the process is that it uses measurements from currently available standard sensors (yaw rate, longitudinal/lateral accelerations, steering angle and angular wheel velocities). Another contribution is that the process provides robust sideslip angle estimations with respect to cornering stiffness changes (or tire-road friction variations). Finally, the estimation process is applied and compared to real experimental data, notably sideslip and wheel force measurements.

The last few years have seen the emergence in cars of active security systems to reduce dangerous situations for drivers. Among these active security systems, Anti-lock Braking Systems (ABS) and Electronic Stability Programs (ESP) significantly reduce the number of road accidents. However, these systems may be improved if the dynamic potential of a car is well known. For example, information on tire-road friction means a better definition of potential trajectories, and therefore a better management of vehicle controls. Nowadays, certain fundamental data relating to vehicle-dynamics are not measurable in a standard car for both technical and economic reasons. As a consequence, dynamic variables such as tire forces and sideslip angle must be observed or estimated.

Vehicle-dynamic estimation has been widely discussed in the literature, e.g. (Kiencke & Nielsen, 2000), (Ungoren et al., 2004), (Lechner, 2002), (Stephant et al., 2006), (Baffet et al, 2006a). The vehicle-road system is usually modeled by combining a vehicle model with a tire-force model in one block. One particularity of this study is that it separates the estimation modeling into two blocks (shown in Figure 1), where the first block concerns the car body dynamic while the second is devoted to the tire-road interface dynamic.

The first block contains an Extended Kalman Filter (denoted as *O1,4w*) constructed with a four-wheel vehicle model and a random walk force model. The first observer *O1,4w* estimates longitudinal/lateral tire forces, velocity and yaw rate, which are inputs to the observer in the second block (denoted as *O2,LAM*). This second observer is developed from a sideslip angle model and a linear adaptive force model.

Source: Advances in Robotics, Automation and Control, Book edited by: Jesús Arámburo and Antonio Ramírez Treviño,
ISBN 78-953-7619-16-9, pp. 472, October 2008, I-Tech, Vienna, Austria

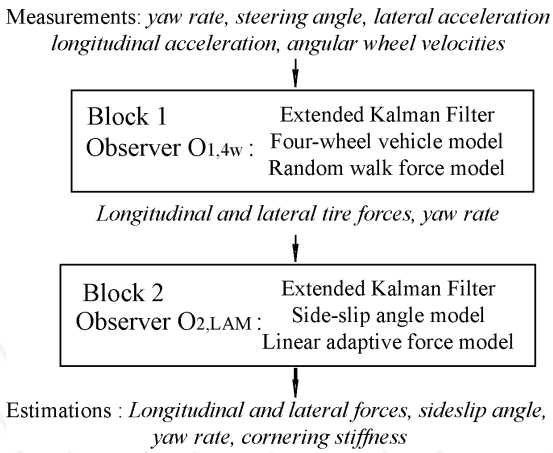

Figure 1. Estimation process. Observers *O1,4w* and *O2,LAM*

Some studies have described observers which take road friction variations into account (Lakehal-ayat et al, 2006), (Rabhi et al, 2005), (Ray, 1997). In the works of (Lakehal-ayat et al, 2006) road friction is considered as a disturbance. Alternatively, as in (Rabhi et al, 2005), the tire-force parameters are identified with an observer, while in (Ray, 1997) tire forces are modeled with an random walk model. In this study a linear adaptive tire force model is proposed (in block 2) with an eye to studying road friction variations.

The rest of the paper is organized as follows. The second section describes the vehicle model and the observer *O1,4w* (block 1). The third section presents the sideslip angle and cornering stiffness observer (*O2,LAM* in block 2). In the fourth section an observability analysis is performed. The fifth section provides experimental results: the two observers are evaluated with respect to sideslip angle and tire-force measurements. Finally, concluding remarks are given in section 6.

2. Block 1: observer for tire-road force

This section describes the first observer *O1,4w* constructed from a four-wheel vehicle model (see Figure 2), where ψ is the yaw angle, β the center of gravity sideslip angle, *Vg* the center of gravity velocity, and *L1* and *L2* the distance from the vehicle center of gravity to the front and rear axles respectively. *Fx,y,i,j* are the longitudinal and lateral tire-road forces, $\delta 1,2$ are the front left and right steering angles respectively, and *E* is the vehicle track (lateral distance from wheel to wheel).

In order to develop an observable system (notably in the case of null steering angles), rear longitudinal forces are neglected relative to the front longitudinal forces. The simplified equation for yaw acceleration (four-wheel vehicle model) can be formulated as the following dynamic relationship (*O1,4w* model):

$$\ddot{\psi} = \frac{1}{I_z}\begin{bmatrix} L_1[F_{y11}\cos(\delta_1) + F_{y12}\cos(\delta_2) + F_{x11}\sin(\delta_1) + F_{x12}\sin(\delta_2)] \\ -L_2[F_{y21} + F_{y22}] \\ E/2[F_{y11}\sin(\delta_1) - F_{y12}\sin(\delta_2) + F_{x12}\cos(\delta_2) - F_{x11}\cos(\delta_1)] \end{bmatrix} \quad (1)$$

where *m* the vehicle mass and *Iz* the yaw moment of inertia. The different force evolutions are modeled with a random walk model:

$$\dot{F_{xij}}, \dot{F_{yij}} = [0,0], \quad i = 1,2, \quad j = 1,2 \tag{2}$$

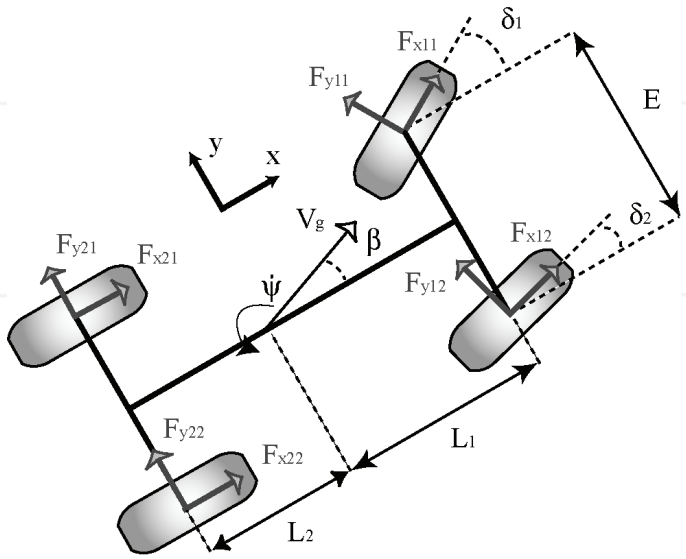

Figure 2. Four-wheel vehicle model

The measurement vector *Y* and the measurement model are:

$$\begin{aligned} Y &= [\dot{\psi}, \gamma_y, \gamma_x] = [Y_1, Y_2, Y_3] \\ Y_1 &= \dot{\psi} \\ Y_2 &= \frac{1}{m}[F_{y11}\cos(\delta_1) + F_{y12}\cos(\delta_2) + F_{y21} + F_{y22} + F_{x11}\sin(\delta_1) + F_{x12}\sin(\delta_2)] \\ Y_3 &= \frac{1}{m}[-F_{y11}\sin(\delta_1) - F_{y12}\sin(\delta_2) + F_{x11}\cos(\delta_1) + F_{x12}\cos(\delta_2)] \end{aligned} \tag{3}$$

where γx and γy are the longitudinal and lateral accelerations respectively.

The *O1,4w* system (association between equations (1), random walk force equation (2), and the measurement equations (3)) is not observable in the case where *Fy21* and *Fy22* are state vector components. For example, in equation (1, 2, 3) there is no relation allowing the rear lateral forces *Fy21* and *Fy22* to be differentiated in the sum *(Fy21+Fy22)*: as a consequence only the sum *(Fy2=Fy21+Fy22)* is observable. Moreover, when driving in a straight line, yaw rate is small, $\delta 1$ and $\delta 2$ are approximately null, and hence there is no significant knowledge in equation (1, 2, 3) differentiating *Fy11* and *Fy12* in the sum *(Fy11+Fy12)*, so only the sum *(Fy1=Fy11+Fy12)* is observable. These observations lead us to develop the *O1,4w* system with a state vector composed of force sums:

$$X = [\dot{\psi}, F_{y1}, F_{y2}, F_{x1}] \tag{4}$$

where *Fx1* is the sum of front longitudinal forces *(Fx1=Fx11+Fx12)*. Tire forces and force sums are associated according to the dispersion of vertical forces:

$$\begin{aligned} F_{x11} &= \frac{F_{z11}}{F_{z11}+F_{z12}} F_{x1,} \quad F_{x12} = \frac{F_{z12}}{F_{z11}+F_{z12}} F_{x1} \\ F_{y11} &= \frac{F_{z11}}{F_{z11}+F_{z12}} F_{y1,} \quad F_{y12} = \frac{F_{z12}}{F_{z11}+F_{z12}} F_{y1} \\ F_{y21} &= \frac{F_{z21}}{F_{z21}+F_{z22}} F_{y2,} \quad F_{y22} = \frac{F_{z22}}{F_{z21}+F_{z22}} F_{y2} \end{aligned} \tag{5}$$

where *Fzij* are the vertical forces. These are calculated, neglecting roll and suspension movements, with the following load transfer model:

$$\begin{aligned} F_{z11} &= \frac{L_2 mg - h_{cog} m\gamma_x}{2(L_1+L_2)} - \frac{L_2 h_{cog} m\gamma_y}{E(L_1+L_2)} \\ F_{z12} &= \frac{L_2 mg - h_{cog} m\gamma_x}{2(L_1+L_2)} + \frac{L_2 h_{cog} m\gamma_y}{E(L_1+L_2)} \\ F_{z21} &= \frac{L_1 mg + h_{cog} m\gamma_x}{2(L_1+L_2)} - \frac{L_1 h_{cog} m\gamma_y}{E(L_1+L_2)} \\ F_{z22} &= \frac{L_1 mg + h_{cog} m\gamma_x}{2(L_1+L_2)} + \frac{L_1 h_{cog} m\gamma_y}{E(L_1+L_2)} \end{aligned} \tag{6}$$

hcog being the center of gravity height and *g* the gravitational constant. The superposition principle means that the load transfer model assumes the assumption of independent longitudinal and lateral acceleration contributions (Lechner, 2002). The input vectors *U* of the *O1,4w* observer corresponds to:

$$U = [\delta_1, \delta_2, F_{z11}, F_{z12}, F_{z21}, F_{z22}] \tag{7}$$

As regards the vertical force inputs, these are calculated from lateral and longitudinal accelerations with the load transfer model.

3. Block 2: observer for sideslip angle and cornering stiffness

This section presents the observer *O2,LAM* constructed from a sideslip angle model and a tire-force model. The sideslip angle model is based on the single-track model (Segel, 1956), with neglected rear longitudinal force:

$$\dot{\beta} = \frac{F_{x1}\sin(\delta-\beta) + F_{y1}\cos(\delta-\beta) + F_{y2}\cos(\beta)}{mV_g} - \dot{\psi} \tag{8}$$

Rear and front sideslip angles are calculated as:

$$\beta_1 = \delta - \beta - L_1 \frac{\dot{\psi}}{V_g}, \quad \beta_2 = -\beta + L_2 \frac{\dot{\psi}}{V_g} \tag{9}$$

where δ is the mean of front steering angles.
The dynamic of the tire-road contact is usually formulated by modeling the tire-force as a function of the slip between tire and road (Pacejka & Bakker, 1991), (Kiencke & Nielsen, 2000), (Canudas-De-Wit et al 2003). Figure 3 illustrates different lateral tire-force models (linear, linear adaptive and Burckhardt for various road surfaces (Kiencke & Nielsen, 2000). In this study lateral wheel slips are assumed to be equal to the wheel sideslip angles.

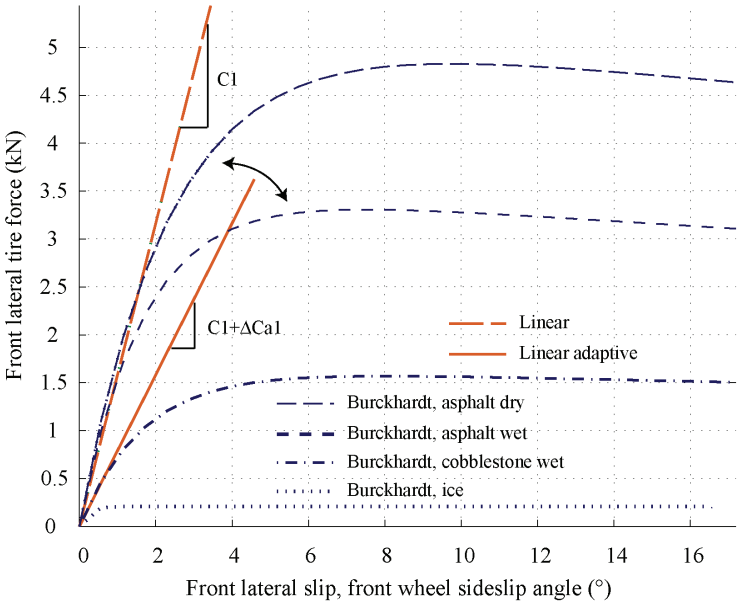

Figure 3. Lateral tire force models: linear, linear adaptive, Burckhardt for various road surfaces

In current driving situations, lateral tire forces may be considered linear with respect to sideslip angle (linear model):

$$F_{yi}(\beta_i) = C_i \beta_i, \quad i = 1,2, \tag{10}$$

where *Ci* is the wheel cornering stiffness, a parameter closely related to tire-road friction.
When road friction changes or when the nonlinear tire domain is reached, "real" wheel cornering stiffness varies. In order a take the wheel cornering stiffness variations into account, we propose an adaptive tire-force model (known as the linear adaptive tire-force model, illustrated in Figure 3. This model is based on the linear model at which a readjustment variable ΔCai is added to correct wheel cornering stiffness errors:

$$F_{yi}(\beta_i) = (C_i + \Delta C_{ai})\beta_i, \quad i = 1,2, \tag{11}$$

The variable ΔCai is included in the state vector of the *O2,LAM* observer and it evolution equation is formulated according to a random walk model. Input *U'*, state *X'* and measurement *Y'* are chosen as:

$$\begin{aligned} U' &= [u_1', u_2', u_3', u_4'] = [\delta, \dot{\psi}, V_g, F_{x1}], \\ X' &= [x_1', x_2', x_3'] = [\beta,\ \Delta C_{a1}, \Delta C_{a2}], \\ Y' &= [y_1', y_2', y_3'] = [F_{y1}, F_{y2}, \gamma_y]. \end{aligned} \tag{12}$$

The measurement model is

$$\begin{aligned} y_1' &= (C_1 + x_2')\beta_1 \\ y_2' &= (C_2 + x_3')\beta_2 \\ y_3' &= \frac{1}{m}((C_1 + x_2')\beta_1 \cos(u_1') + (C_2 + x_3')\beta_2 + u_4' \sin(u_1')) \end{aligned} \tag{13}$$

where

$$\begin{aligned} \beta_1 &= u_1' - x_1' - L_1 {u_2'}/{u_3'} \\ \beta_2 &= -x_1' + L_2 {u_2'}/{u_3'} \end{aligned} \tag{14}$$

Given the state estimation denoted as

$$X' = [x_1', x_2', x_3'] \tag{15}$$

the state evolution model of *O2,LAM* is:

$$\begin{aligned} \dot{x_1}' &= \frac{1}{m u_3}[u_4 \sin(u_1 - x_1') + F_{yw1aux} \cos(u_1' - x_1') + F_{yw2aux} \cos(x_1') - u_2'] \\ \dot{x_2}' &= 0 \\ \dot{x_3}' &= 0 \end{aligned} \tag{16}$$

where the auxiliary variables *Fyw1,aux* and *Fyw2,aux* are calculated as:

$$\begin{aligned} F_{yw1,aux} &= (C_1 + x_2')(u_1' - x_1' - L_1 {u_2'}/{u_3'}) \\ F_{yw2,aux} &= (C_2 + x_3')(-x_1' + L_2 {u_2'}/{u_3'}) \end{aligned} \tag{17}$$

4. Estimation method

The different observers (*O1,4w*, *O2,LAM*) were developed according to an extended Kalman filter method. In 1960 R. E. Kalman published a paper describing a recursive solution to the discrete-data linear filtering problem (Kalman, 1960). Since this publication, Kalman's method, usually known as the "Extended Kalman Filter", has been the object of extensive

search and numerous applications. For example, in (Mohinder & Angus, 1993), Mohinder and Angus present a broad overview of Kalman filtering.
This paragraph describes an EKF algorithm. *bs,k*, *be,k* and *bm,k* represent measurement noise at time *tk* for the measurements, inputs and state evolution model respectively. This noise is assumed to be Gaussian, white and centered. *Qs*, *Qe* and *Qm* are the noise variance-covariance matrices for *bs,k*, *be,k* and *bm,k*, respectively. The discrete form of models is:

$$\begin{aligned} \mathrm{F}(\mathrm{X}_k, U_k^*) &= X_k + \int_{t_k}^{t_{k+1}} f(X_k, U_k^*)dt \\ X_{k+1} &= \mathrm{F}(\mathrm{X}_k, U_k^*) + b_{m,k} \\ Y_k &= h(\mathrm{X}_k, U_k^*) + b_{s,k} \\ U_k^* &= U_k + b_{e,k} \end{aligned} \tag{18}$$

where f and h are the evolution and measurement functions. X_k^- and X_k^+ are state prediction and estimation vectors, respectively, at time *tk*. The first step of the EKF is to linearize the evolution equation around the estimated state and input:

$$\begin{aligned} A_k &= \frac{\partial F}{\partial X}\left(X_k^+, U_k^*\right) \\ B_k &= \frac{\partial F}{\partial U}\left(X_k^+, U_k^*\right) \end{aligned} \tag{19}$$

The second step is the prediction of the next state, from the previous state and measured input:

$$X_{k+1}^- = F\left(X_k^+, U_k^*\right) \tag{20}$$

The covariance matrix of state estimation uncertainty is then:

$$P_{k+1}^- = A_k P_k^+ A_k^\perp + B_k Q_e B_k^\perp + Q_m \tag{21}$$

The third step is to calculate the Kalman gain matrix from the linearization of the measurement matrix:

$$\begin{aligned} C_k &= \frac{\partial h}{\partial X}\left(X_{k+1}^-, U_k^*\right) \\ B_k &= \frac{\partial F}{\partial U}\left(X_{k+1}^-, U_k^*\right) \\ D_k &= \frac{\partial h}{\partial U}\left(X_{k+1}^-, U_k^*\right) \end{aligned} \tag{22}$$

The following intermediate variables are used:

$$\begin{aligned} R_k &= C_k P_{k+1}^- C_k^\perp + D_k Q_e D_k^\perp \\ S_k &= B_k Q_e D_k^\perp \\ T_k &= P_{k+1}^- C_k^\perp + S_k \end{aligned} \tag{23}$$

and the Kalman gain matrix is:

$$K_k = T_k(R_k + Q_s + C_k S_k + S_k^{\perp} C_k^{\perp})^{-1} \tag{24}$$

The estimation step is to correct the state vector in line with measurement errors:

$$X_{k+1}^{+} = X_{k+1}^{-} + K_k\left[Y_{k+1} - h\left(X_{k+1}^{-}, U_{k+1}^{*}\right)\right] \tag{25}$$

Finally, the covariance matrix of state estimation uncertainty becomes:

$$P_{k+1}^{+} = P_{k+1}^{-} - K_k(C_k P_{k+1}^{-} + S_k^{\perp}) \tag{26}$$

5. Observability

From the two vehicle-road systems (*O1,4w*, *O2,LAM*), two observability functions were calculated. The two systems are nonlinear, so the observability definition is local and uses the Lie derivative (Nijmeijer & Van der Schaft 1990).
The Lie derivative of *hi* function, at *p+1* order, is defined as:

$$L_f^{p+1} h_i = \frac{\partial L_f^p h_i(X)}{\partial X} f(X,U) \tag{27}$$

With

$$L_f^1 h_i(X) = \frac{\partial h_i(X)}{\partial X} f(X,U) \tag{28}$$

The observability function *oi* corresponding to the measurement function *hi* is defined as:

$$o_i = \begin{pmatrix} dh_i(X) \\ dL_f^1 h_i(X) \\ \dots \\ dL_f^{(n-1)} h_i(X) \end{pmatrix} \tag{29}$$

where *n* is the dimension of *X* vector and *d* is the operator:

$$dh_i = \left(\frac{\partial h_i}{\partial x_1}, \dots, \frac{\partial h_i}{\partial x_6}\right) \tag{30}$$

The observability function of the system is calculated as:

$$O = \left(o_1, \dots, o_p\right)^{\perp} \tag{31}$$

where *p* is the dimension of the *Y* vector. Figure 4 illustrates observability analysis of the two systems for an experimental test, presented in section 6**.** Ranks of the two observability functions were 4 (for *O1,4w*) and 3 (for *O2,LAM*) (state dimensions) throughout the test, and consequently the state of the two systems were locally observable.

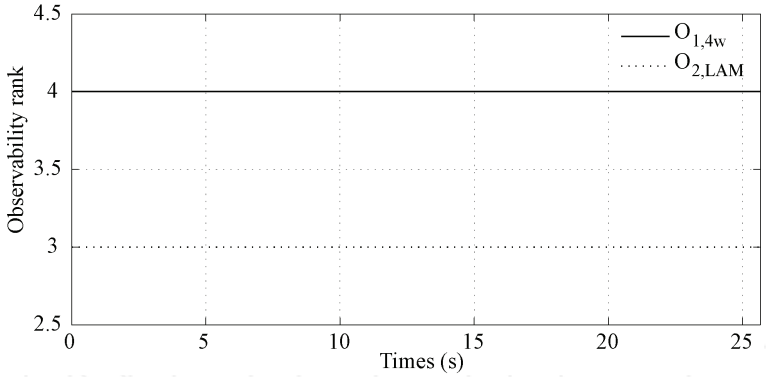

Figure 4. Ranks of the two observability functions for systems O1,4w and O2,LAM, during an experimental test (slalom)

6. Experimental results

The experimental vehicle (see Figure 5) is a Peugeot 307 equipped with a number of sensors including GPS, accelerometer, odometer, gyrometer, steering angle, correvit and dynamometric hubs. Among these sensors, the correvit (a non-contact optical sensor) gives measurements of rear sideslip angle and vehicle velocity, while the dynamometric hubs are wheel-force transducers.

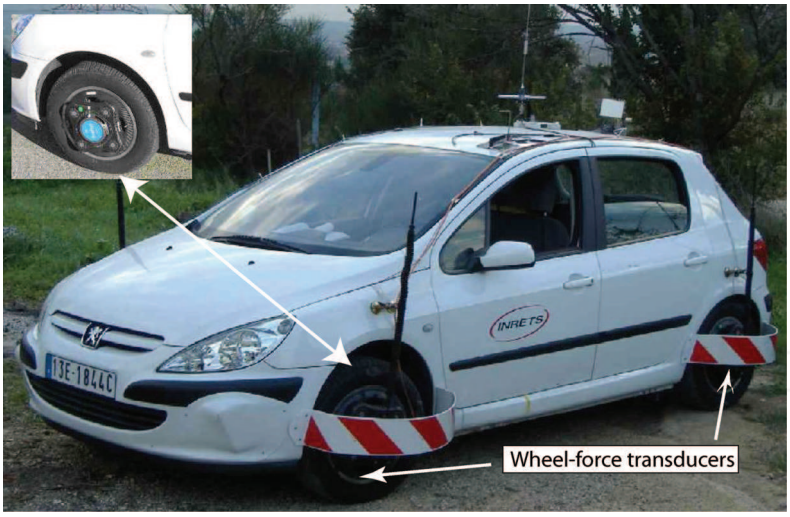

Figure 5. Laboratory's experimental vehicle

This study uses an experimental test representative of both longitudinal and lateral dynamic behaviors. The vehicle trajectory and the acceleration diagram are shown in Figure 6. During the test, the vehicle first accelerated up to $\gamma x \approx 0.3g$, then negotiated a slalom at an approximate velocity of *12 m/s* ($-0.6g < \gamma y < 0.6g$), before finally decelerating to $\gamma x \approx 0.7g$.

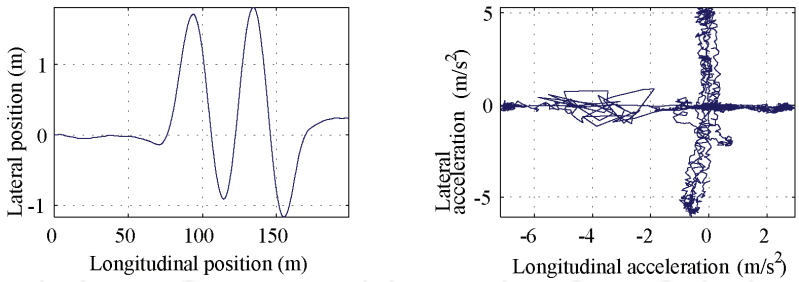

Figure 6. Experimental test, vehicle positions, acceleration diagram

The results are presented in two forms: figures of estimations/measurements and tables of normalized errors. The normalized error εz for an estimation z is defined in (Stephant et al, 2006) as

$$\varepsilon_z = 100 \frac{|z - z_{measurement}|}{|\max(z_{measurement})|} \tag{32}$$

6.1 Block 1: observer O1,4w results

Figure 7 and table 1 present *O1,4w* observer results.

Estimates	Max	Mean	Std
$\dot{\psi}$	24.6°/s	0.4 %	2.6 %
Fy1	5816 N	3.1 %	4.0 %
Fy2	3782 N	2.9 %	5.4 %
Fx1	9305 N	3.1 %	4.1 %

Table 1. Maximum absolute values, *O1,4w* normalized mean errors and normalized standard deviation (Std)

The state estimations were initialized using the maximum values for the measurements during the test (for instance, the estimation of the front lateral force *Fy1* was set to *5155 N*). In spite of these false initializations the estimations converge quickly to the measured values, showing the good convergence properties of the observer. Moreover, the *O1,4w* observer produces satisfactory estimations close to measurements (normalized mean and standard deviations errors are less than *7 %*). These good experimental results confirm that the observer approach may be appropriate for the estimation of tire-forces.

6.2 Block 2: observer O2,LAM results

During the test, (*Fx1, Fy1, Fy2, Vg*) inputs of *O2,LAM* were originally those from the *O1,4w* observer. In order to demonstrate the improvement provided by the observer using the *linear adaptive force model* (*O2,LAM*, equation 11), another observer constructed with a *linear fixed force model* is used in comparison (denoted *Orl*, equation 10, described in (Baffet et al, 2006b). The robustness of the two observers is tested with respect to tire-road friction variations by performing the tests with different cornering stiffness parameters (*[C1, C2]*0.5, 1, 1.5*). The observers were evaluated for the same test presented in section 6.

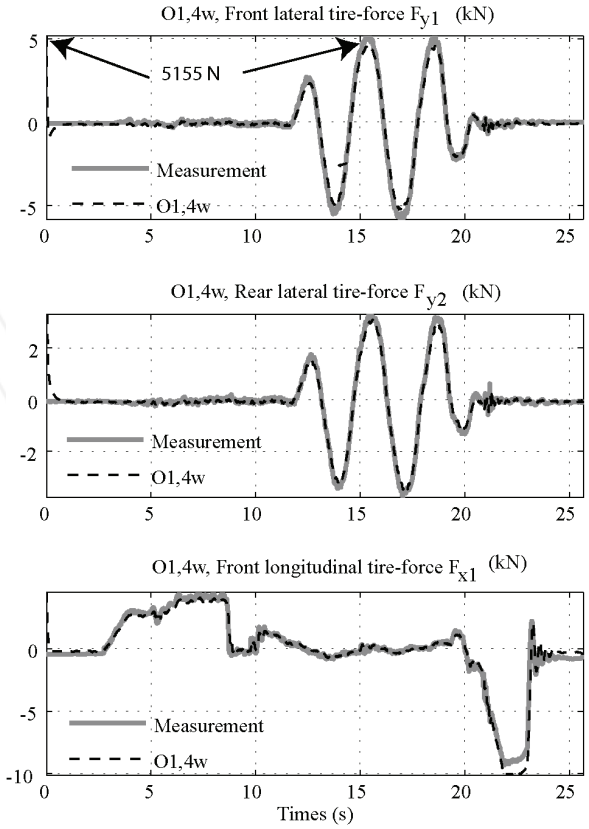

Figure 7. Experimental test. O1,4w results in comparison with measurements.Figure 8 shows the estimation results of observer *Orl* for rear sideslip angle. Observer *Orl* gives good results when cornering stiffnesses are approximately known (*[C_1, C_2]*1*). However, this observer is not robust when cornering stiffnesses change (*[C_1, C_2]*0.5, 2*).

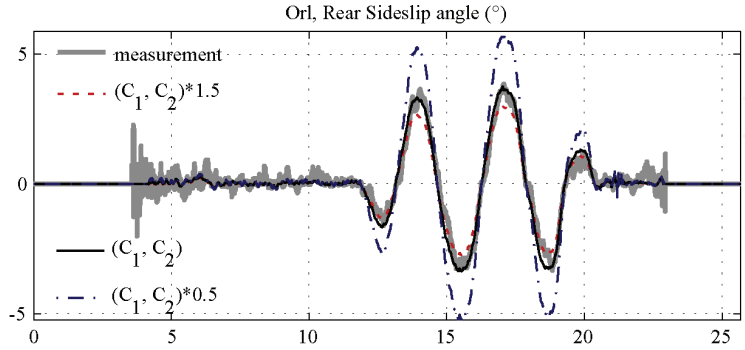

Figure 8. Observer Orl using a fixed linear force model, rear sideslip angle estimations with different cornering stiffness settings.

Figure 9 and table 2 show estimation results for the adaptive observer *O2,LAM*. The performance robustness of *O2,LAM* is very good, since sideslip angle is well estimated irrespective of cornering stiffness settings. This result is confirmed by the normalized mean errors (Table 2) which are approximately constant (about *7 %*). The front and rear cornering stiffness estimations (Ci + ΔCi) converge quickly to the same values after the beginning of the slalom at *12 s*.

O2,LAM	0.5(C1,C2)	(C1,C2)	1.5(C1,C2)
Max	3.0°	3.0°	3.0°
Mean	7.4 %	7.0 %	7.2 %

Table 2. Observer *O2,LAM*, rear sideslip angle estimation results, maximum absolute value, normalized mean errors.

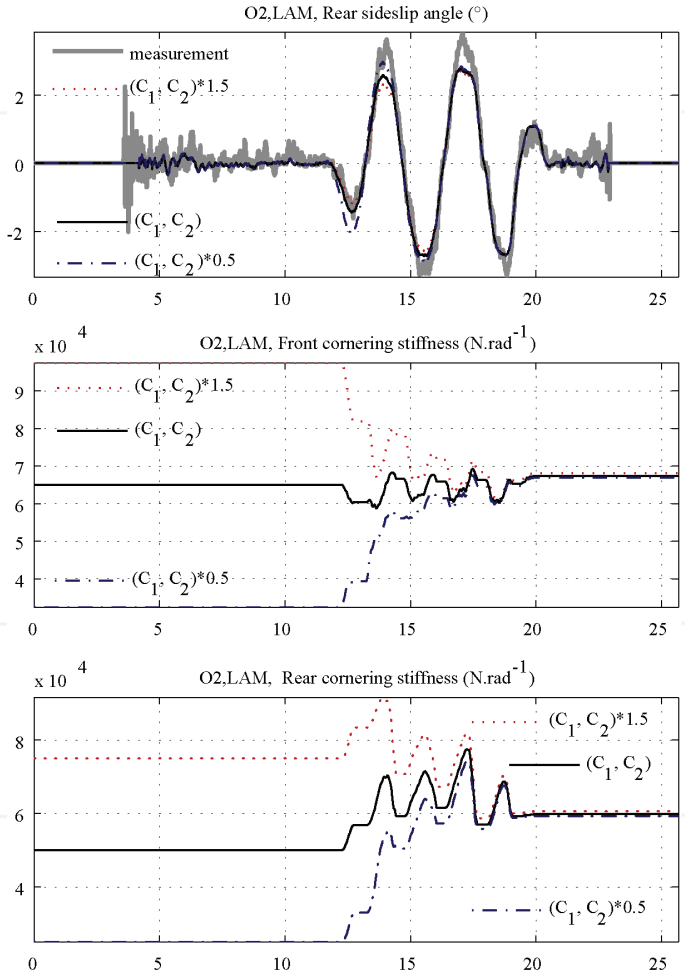

Figure 9. O2,LAM adaptive observer, Sideslip angle estimation results, Front and rear cornering stiffness estimations Ci+ ΔCi, with different cornering stiffness settings

6. Conclusions

This study deals with two vehicle-dynamic observers constructed for use in a two-block estimation process. Block 1 mainly estimates tire-forces (without an explicit tire-force model), while block 2 calculates sideslip angle and corrects cornering stiffnesses (with an adaptive tire-force model).

The first observer *O1,4w* (block 1), an extended Kalman Filter, is constructed with a random walk force model. The experimental evaluations of *O1,4w* are satisfactory, showing excellent estimations close to the measurements and good convergence properties.

The second observer *O2,LAM* (block 2), developed with an adaptive tire-force model, was evaluated for different cornering stiffness settings and was compared with an observer constructed with a fixed tire-force model (Orl). Results show that Orl is not robust when cornering stiffness parameters change, whereas *O2,LAM* gives excellent estimations of the sideslip angle. This result justifies the use of an adaptive tire-force model to take into account road friction changes.

The different results show the potential of the two-block estimation process. The first block has the advantage of providing satisfactory force estimations without a tire-force model, whereas the second block provides robust sideslip angle estimations with respect to cornering stiffness changes (or tire-road friction variations).

Future studies will improve vehicle-road models, notably for the calculation of the front/rear sideslip angles, in order to widen validity domains for observers. Subsequent vehicle-road models will take into account roll, vertical dynamics and vehicle-tire elasto-kinematics. Moreover, experimental tests will be performed, notably on different road surfaces and in critical driving situations (strong understeering and oversteering).

7. References

Baffet, G.; Stephant, J. & Charara, A. (2006). Vehicle Sideslip Angle and Lateral Tire-Force Estimations in Standard and Critical Driving Situations: Simulations and Experiments. *Proceedings of the 8th International Symposium on Advanced Vehicle Control AVEC2006*, pp 41-45, Taipei Taiwan

Baffet, G.; Stephant, J. & Charara, A. (2006). Sideslip angle lateral tire force and road friction estimation in simulations and experiments. *Proceedings of the IEEE conference on control application CCA,* pp. 903-908, Munich, Germany

Bolzern, P.; Cheli, F.; Falciola, G. & Resta, F. (1999). Estimation of the nonlinear suspension tyre cornering forces from experimental road test data. *Vehicle system dynamics.* Vol.31, 23-34

Canudas-De-Wit, C.; Tsiotras, P.; Velenis, E.; Basset, M. & Gissinger, G. (2003). Dynamic friction models for road/tire longitudinal interaction. *Vehicle System Dynamics,* Vol.39, 189-226

Kalman, R.E. (1960). A New Approach to Linear Filtering and Prediction Problems. *Transactions of the ASME - PUBLISHER of Basic Engineering,* Vol.82, 35-45

Kiencke U. & Nielsen, L. (2000). *Automotive control system.* Springer

Lakehal-ayat, M.; Tseng, H.E.; Mao, Y. & Karidas, J. (2006). Disturbance Observer for Lateral Velocity Estimation. *Proceedings of the 8th International Symposium on Advanced Vehicle Control AVEC2006,* pp 889-894, Taipei Taiwan

Lechner, D. (2002). *Analyse du comportement dynamique des vehicules routiers legers: developpement d'une methodologie appliquee a la securite primaire.* Ph.D. dissertation Ecole Centrale de Lyon, France

Mohinder, S.G. & Angus, P.A. (1993) *Kalman filtering theory and practice.* Prentice hall.

Nijmeijer, H. & Van der Schaft, A.J. (1990) *Nonlinear Dynamical Control Systems.* Springer-Verlag

Pacejka, H.B. & Bakker, E. (1991). The magic formula tyre model. *Int. colloq. on tyre models for vehicle dynamics analysis,* 1-18

Rabhi, A. ; M'Sirdi, N.K. ; Zbiri, N. & Delanne, Y (2005). Vehicle-road interaction modelling for estimation of contact forces. *Vehicle System Dynamics,* Vol.43, 403-411

Ray, L. (1997). Nonlinear Tire Force Estimation and Road Friction Identification : Simulation and Experiments. *Automatica,* Vol.33, 1819-1833

Segel, M.L. (1956). Theorical prediction and experimental substantiation of the response of the automobile to steering control. *Automobile division of the institut of mechanical engineers*, Vol.7, 310-330

Stephant, J.; Charara, A. & Meizel, D. (2006). Evaluation of a sliding mode observer for vehicle sideslip angle. *Control Engineering Practice*, Vol. 15, 803-812

Ungoren, A.Y.; Peng, H. & Tseng, H.E. (2004). A study on lateral speed estimation methods. *Int. J. Vehicle Autonomous Systems,* Vol.2, 126-144

Advances in Robotics, Automation and Control

Edited by Jesus Aramburo and Antonio Ramirez Trevino

ISBN 978-953-7619-16-9
Hard cover, 472 pages
Publisher InTech
Published online 01, October, 2008
Published in print edition October, 2008

The book presents an excellent overview of the recent developments in the different areas of Robotics, Automation and Control. Through its 24 chapters, this book presents topics related to control and robot design; it also introduces new mathematical tools and techniques devoted to improve the system modeling and control. An important point is the use of rational agents and heuristic techniques to cope with the computational complexity required for controlling complex systems. Through this book, we also find navigation and vision algorithms, automatic handwritten comprehension and speech recognition systems that will be included in the next generation of productive systems developed by man.

How to reference

In order to correctly reference this scholarly work, feel free to copy and paste the following:

Guillaume Baffet, Ali Charara and Daniel Lechner (2008). Estimation of Tire-Road Forces and Vehicle Sideslip Angle, Advances in Robotics, Automation and Control, Jesus Aramburo and Antonio Ramirez Trevino (Ed.), ISBN: 978-953-7619-16-9, InTech, Available from: http://www.intechopen.com/books/advances_in_robotics_automation_and_control/estimation_of_tire-road_forces_and_vehicle_sideslip_angle

INTECH
open science | open minds

InTech Europe
University Campus STeP Ri
Slavka Krautzeka 83/A
51000 Rijeka, Croatia
Phone: +385 (51) 770 447
Fax: +385 (51) 686 166
www.intechopen.com

InTech China
Unit 405, Office Block, Hotel Equatorial Shanghai
No.65, Yan An Road (West), Shanghai, 200040, China
中国上海市延安西路65号上海国际贵都大饭店办公楼405单元
Phone: +86-21-62489820
Fax: +86-21-62489821